Topological quantum criticality of the disordered Chern insulator

Mateo Moreno-Gonzalez

Institute for theoretical physics, Universität zu Köln, Zülpicher Str. 77a, 50937 Cologne, Germany

Johannes Dieplinger

Institute for theoretical physics, Universität Regensburg, 93040 Regensburg, Germany

Alexander Altland

Institute for theoretical physics, Universität zu Köln, Zülpicher Str. 77a, 50937 Cologne, Germany

We consider the two-dimensional topological Chern insulator in the presence of static disorder. Generic quantum states in this system are Anderson localized. However, topology requires the presence of a subset of critical states, with diverging localization length (the Chern insulator analog of the 'center of the Landau band states' of the quantum Hall insulator.) We discuss geometric criteria for the identification of these states at weak disorder, and their extension into the regime of strong disorder by analytical methods. In this way, we chart a critical surface embedded in a phase space spanned by energy, topological control parameter, and disorder strength. Our analytical predictions are supplemented by a numerical analysis of the position of the critical states, and their multifractal properties.

I. INTRODUCTION

Next to the one-dimensional SSH chain the quantum anomalous Hall insulator (aka Chern insulator) is the most basic topological insulator. Defined in two dimensions, the system does not possess symmetries other than hermiticity of the Hamilitonian (class A). It is 'anomalous' in that its topological order is intrinsic, and does require an external magnetic field as in the conventional quantum Hall insulator. (In fact, the first theoretical model of a AQH insulator was proposed by Haldane [1] as a 'field free' realization of a quantum Hall effect.)

In the presence of static disorder, the AQH band insulator turns into a topological Anderson insulator [2, 3], and the spectral band gap becomes a mobility gap. Crucially, however, at least some of its states must remain delocalized. As with the critically delocalized states in the center of the IQH Landau levels, the presence of such states is required for consistency. If there were not any, one would end up with contradictions such as vanishing of the *transverse* Hall conductance, whose integer quantization is the defining feature of this system [4]. Alternatively one may reason that the band of conducting surface states cannot simply disappear but must hybridize with states from the other surface somewhere up in the spectrum via delocalized bulk states.

However, to the best of our knowledge the physics of AQH state delocalization has not yet been systematically explored. Is there a single energy at which states delocalize and if yes, where in the band is it situated? How much disorder is required to destroy the delocalized states, and in this way the topological phase at large? What are the critical properties of the delocalized states and how do they compare to those of the IQH Landau level center states? In this paper, we address these questions within a two-thronged approach combining field theoretical constructions with high performance direct diagonalization.

Indeed it turns out that analytical methods go a long way in the characterization of AQH delocalized states. The main result will be a phase diagram spanned by three parameters. The first is a parameter, r, controlling the topological properties, i.e. the topological index, $\nu(r) \in \mathbb{Z}$, of the clean system. The second is band energy, E, and the third the disorder strength, W. Embedded in this parameter space there lies a two dimensional surface, whose crossing implies criticality and along with it the divergence of correlation lengths, or 'delocalization', see Fig.1 for a schematic. For example, for $E = 0$, the critical line $W(r)$, marks a stability boundary at which disorder enforces a phase transition between the topological and a trivial insulator. The critical value $E(r, W)$ defines the value in energy at which state delocalize for a given control parameter and disorder strength, etc.

At weak disorder, the dependence $E(r, W)$ is encoded in the ground state of the clean topological insulator. (Specifically, we will show that for a simple two-band model of the Chern insulator, the critical state is defined by a half-integer Berry flux quantization condition.) For stronger disorder, the computation of the critical energy gets a little more involved, but even then requires no more than knowledge of the SCBA Green function, i.e. $G(z) = (z - H(k) - \Sigma)^{-1}$, where $H(k)$ is the clean Hamiltonian, and Σ the average quasiparticle self energy due to impurity scattering. The condition for criticality then follows via computation of a few integrals of Green functions over the Brillouin zone, which may be done analytically, or numerically.

The result of this analysis is a comprehensive phase portrait of the disordered Chern insulator, including predictions for its stability boundaries, the critical states, and conduction properties at finite system sizes before Anderson localization becomes effective in the thermodynamic limit.

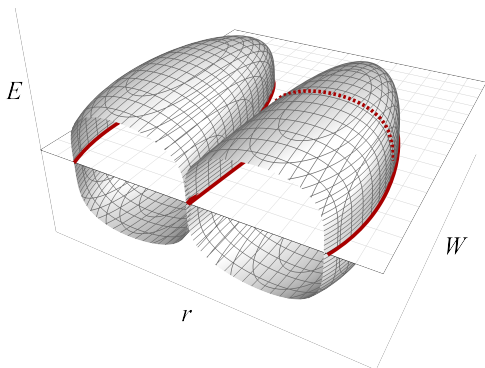In the next section, we summarize the main results of

FIG. 1. Schematic illustration of the critical surface of a Chern insulator. The clean system is defined in terms of different topological sectors realized as a function of a control parameter r, for example, $Ch_1 = 0 \to 1 \to -1 \to 0$. For a given value of r and disorder strength, W, delocalized states exist at a critical energies $E_l(r, W)$, one for each band. The merging of these bands at the center of the spectrum marks the stability boundary of the TI; for larger disorder the system has become a trivial Anderson insulator. (For systems with high Chern indices, $\max|Ch_l| > 1$, the destruction of topological order for increasing W occurs in the successive merging of multiple surfaces $E_l(r, W)$.)

our study. This will be followed by section III where we present a self contained derivation of the topological field theory underlying our analytical results. In section IV we discuss the results obtained from both, the numerical and analytical calculations and we conclude in section V.

II. SUMMARY OF RESULTS

We begin this section with a short review of the clean Chern insulator. This will be followed by the discussion of an effective field theory describing the critical physics of the disordered system, and a comparison to the conventional quantum Hall insulator. We conclude with a discussion of numerical results.

A. Clean Chern insulator

The clean two-dimensional (more generally, even-dimensional) Chern insulator is a topological insulator characterized by non-vanishing Chern number, Ch_l, carried by individual of its bands, $l = 1, \ldots, N$. These numbers are constructed from the Berry connection $a = i\langle k|dk\rangle = i\langle k|\partial_{k_i}k\rangle dk_i$, where $\{|k\rangle\}$ are the Bloch eigenstates of a specific band, and $k = (k_1, k_2)$ is crystal momentum [5–7]. Integration of the Berry curvature $b = da = i\langle \partial_{k_j}k|\partial_{k_i}k\rangle dk_i \wedge dk_j$ over the Brillouin zone then yields the Chern number as, $Ch_l = \frac{1}{4\pi}\int_{BZ} b$.

The simplest model system realizing a nontrivial set of Chern numbers is Haldane's two-band QAH insulator

[1, 8], defined by the Hamiltonian

$$H = \sin k_1 \sigma_1 + \sin k_2 \sigma_2 + (r - \cos k_1 - \cos k_2)\sigma_3$$

$$\equiv \sum_{a=1}^{3} h_a(k)\sigma_a, \tag{1}$$

where we have set the hopping strength to unity for simplicity. For $r \neq -2, 0, 2$ this is a two-band insulator with 'valence' and 'conduction' band Chern numbers $(Ch_v, Ch_c) = (0,0), (-1,1), (1,-1), (0,0)$ for $r < -2, -2 < r < 0, 0 < r < 2, 2 < r$, respectively. In this particular case, the integral over the Berry curvature assumes the form $Ch_c = -Ch_v = \frac{1}{4\pi}\int d^2k\, n\cdot(\partial_{k_1}n \times \partial_{k_2}n))$, where $n = h/|h|$, i.e. it probes the number of windings of the Pauli vector $h = \{h_a\}$ defining the Hamiltonian over the unit sphere.

B. Disordered Chern insulator

In the presence of translational invariance breaking disorder, the Bloch eigenstates of the system get replaced by states which generically are Anderson localized. For impurity scattering rates, τ^{-1}, comparable to the band gap of the clean system, the spectral gap gets filled by impurity states, with a globally gapless spectral density. The topological properties of the system, too, are no longer characterized by momentum space invariants but instead by a effective field theory defined in real space.

To define this theory, consider the matrix $Q = T\tau_3 T^{-1}$, where $T \in U(2R)$ is a unitary matrix, R a number of replicas $(R \to 0$, eventually), and the doubling factor 2 required to distinguish between retarded and advanced Green functions in the computation of observables in this formalism. The matrix $\tau_3 = \tau_3 \otimes \mathbb{1}_R$ acts in this space, and its presence implies that $Q \in U(2R)/U(R) \times U(R)$ is element of a coset space in which matrices commutative with τ_3 are divided out.

Promoting $Q = Q(x)$ to a matrix field defined in two-dimensional space, we note that there are just two rotationally invariant gradient operators. They define an effective action as

$$S[Q] = \int d^2x \left(g\, tr(\partial_i Q \partial_i Q) + \frac{\theta}{16\pi}\epsilon_{ij}\, tr(Q\partial_i Q \partial_j Q) \right), \tag{2}$$

where the two coupling constants $g = \sigma_{xx}/8$ and $\theta = 2\pi\sigma_{xy}$ are determined by the system's longitudinal and transverse Hall conductance, respectively (in units of the conductance quantum).

The second term in Eq. (2) is topological in nature. For a fictitious infinitely extended (or boundary-less) system it computes $(16\pi i \times)$ the number of times $Q(x)$ covers the coset space $U(2R)/U(R) \times U(R)$ as a function of x. In its absence fluctuations of the Q-matrix field will lead to a logarithmically slow downward renormalization of $g \sim \sigma_{xx}$ — two-dimensional Anderson localization [9].

The same happens for generic values of $\theta \sim \sigma_{xy}$. In fact, Pruisken [10, 11] derived the above action as the effective theory underlying Khmelnitskii's two parameter scaling paradigm [12] according to which the flow of coupling constants $(g, \theta) \to (0, 2\pi n)$ generically ends in localizing fixed points, $g = 0$, with integer quantized Hall conductance, $\sigma_{xy} = n$.

The exceptional situation occurs at $\theta = \pi$. For this critical value the flow ends in a fixed point with finite conductance, (g^*, π), the quantum Hall critical point. (The critical point itself is described by an effective theory different from Eq. (2). While the identity of that theory remains unknown to date, our focus here is on the identification of criticality, and for that purpose Eq. (2) remains the appropriate diagnostic.)

The identification of the phases supported by a two-dimensional class A topological insulator thus amounts to the computation of the parameters (g, θ) for a given microscopic system description. Previous work [13] performed this task in a Dirac or '$k \cdot p$' approximation, valid for energies close to a band closing point. Since, however, the critical surfaces may be buried deeply in the Chern bands, this approximation is not an option here, we need to work with the full lattice dispersion. Interestingly, abandoning the Dirac linearization turns out to be a blessing, including from a computational perspective: the construction of effective field theories building on top of a microscopic Dirac Hamiltonian is met with ultraviolet singularities. These need to be regularized by one of various available schemes, which, however, are all *ad-hoc* from a condensed matter perspective [14–16]. However, these singularities are a mere artifact of the linearization, they do not occur within for the full system with its bounded dispersion relations. Relatedly, they obscure the geometric interpretation of the topological angle as an integral over the Brillouin zone.

In section III, we will see that the derivation of the effective theory building on the lattice Hamiltonian is both more general and conceptually simpler than the Dirac approach. Specifically, it yields the topological angle at weak disorder of the two-band insulator as an integral

$$\theta = \frac{1}{2} \int_{\epsilon_k > E} d^2k \, n \cdot (\partial_{k_1} n \times \partial_{k_2} n)). \tag{3}$$

While this expression is derived for the simplest model of a Chern insulator, the generalization to others is obvious: the topological angle is defined by the fraction of the full Berry flux $2\pi l$ carried by all states in the band above the reference energy E (Since only $\theta \bmod 2\pi$ matters, we may equally compute the flux of states below E). Criticality occurs for states for which $\theta(E) = \pi$.

Far from the weak disorder the fractional Berry flux becomes statistically distributed, and its mean value features as the topological angle θ. This value can be represented as the sum of two momentum space integrals over SCBA broadened Green functions, aka the Smrčka-Středa coefficients [17], $\theta^{\mathrm{I}} = 2\pi \sigma_{xy}^{\mathrm{I}}$ and $\theta^{\mathrm{II}} = 2\pi \sigma_{xy}^{\mathrm{II}}$. Odd integer values $\theta = \theta^{\mathrm{I}} + \theta^{\mathrm{II}} = (2n+1)\pi$ serve as markers for

topological quantum criticality, as in the IQH context.

C. Numerical analysis of the multifractal spectrum

Complementing the analytical approach, we diagnose criticality numerically via multifractal analysis of states at the critical points [18–21]. Our starting point is the tight-binding model in Eq. (1) with periodic boundary conditions and on-site uncorrelated Gaussian disorder with width W. For a given wave function ψ_E at energy E, the key objects of interest are the q-th moments

$$P_q^E = \sum_{ij}^{N} \sum_{\alpha} \mid \psi_{ij,\alpha}^E \mid^{2q}, \tag{4}$$

where $\psi_{ij,\alpha}^E$ labels the wave function element at lattice site (i, j) and internal degree of freedom $\alpha = 1, 2$.

Th q-th of these moments scales with linear system size N as

$$P_q^E(N) \propto N^{\tau_q}, \tag{5}$$

where τ_q is the effective dimension. Extended metallic wave functions in a d-dimensional lattice have dimension $\tau_q^{\mathrm{metal}} = d(q - 1)$, while localized wave function show system size independent scaling $\tau_q^{\mathrm{loc}} = 0$. Finally, the fluctuations of a critical wave function are captured by the anomalous part of the effective dimension [18, 20],

$$\Delta_q^E = \tau_q^E + d(q - 1). \tag{6}$$

Specifically, the multifractal dimension of the quantum Hall transition has an approximately parabolic spectrum with $\Delta_q^{\mathrm{QH}} \approx 0.25\, q\, (q - 1)$[22]. Below, we will use this scaling as a benchmark for diagnosing quantum Hall criticality in the Chern insulator.

In practice we calculate the quantity

$$\tilde{\tau}_q(N; E, W, r) = \frac{\log \langle P_q^{E,W,r}(N) \rangle_{\mathrm{dis,E}}}{\log N}, \tag{7}$$

where $\langle \cdot \rangle_{\mathrm{dis,E}}$ denotes the double average over a small energy window, consisting of N_E subsequent wave functions as well as over N_{avg} disorder configurations. In the limit of infinite system size, $\lim_{N \to \infty} \tilde{\tau}_q(N) = \tau_q$.

In Fig. 2 we show $\tilde{\tau}_{0.5}$ close to the critical surface for fixed r, E for different W. The critical state is identified as the maximum of the data for a given system size N. Finite size scaling and extrapolation to $N \to \infty$ allows us to extract the limiting effective dimension τ_q, the critical disorder strength at this system parameters, and the localization length exponent ν. Referring for details of the extrapolation procedure to Appendix F, we also extract the corresponding irrelevant scaling corrections y_τ, y_ν from the curvature of the data for different system sizes.

Fig. 3 shows the scaling of the extrapolated critical exponents. We find $\tau_{0.5} = 0.931 \pm 0.004$, $\nu = 2.73 \pm 0.16$.
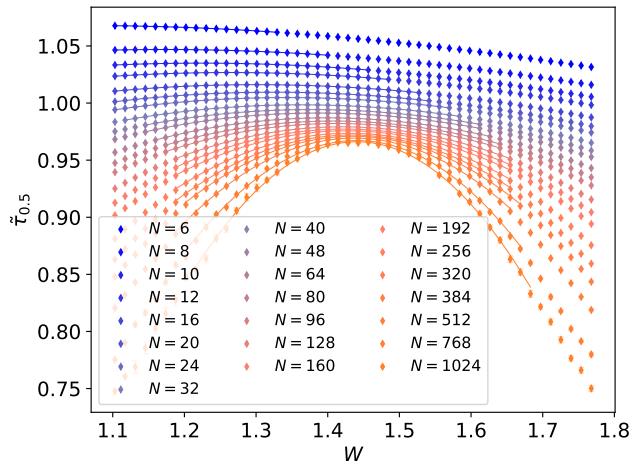
FIG. 2. Effective dimension $\tilde{\tau}_q(E, W, r)$ for different system sizes at the point $(r, E) = (1.2, 0.6)$ as a function of W. The data is approximately described by parabolas with increasing opening angle for increasing system size. The fit (solid lines) is done using a cubic polynomial Eq. (F1) to account for asymmetries away from the critical point.

Within the error bars this is consistent with results for the integer quantum Hall effect in Chalker-Coddington networks and tight binding models [23–26].

The above discussion shows that field theory and numerical analysis provide complementary means to identify and analyze the critical state of the Chern insulator. In particular, one can be used to test the accuracy of the other. (We will see, that this validation goes in both directions.) Referring to section IV for the detailed comparison, we will identify the position of the extended state in the conduction band given r and W, and on this identify a phase boundary in the $r - W$ at the band center $E = 0$. Building on this information, we will then map out the full phase diagram in (r, W, E) space. However, before turning to this comparison, we include a self contained discussion of the field theoretical apparatus underlying our results. This section may be skipped by readers primarily interested in results.

III. DERIVATION OF THE EFFECTIVE ACTION

In this section we discuss the derivation of the effective action Eq. (2) of the disordered Chern insulator. While the initial steps of the construction are standard, they are included here to keep the discussion self contained. Emphasis will then be put on the derivation of the topological action, which is technically novel.
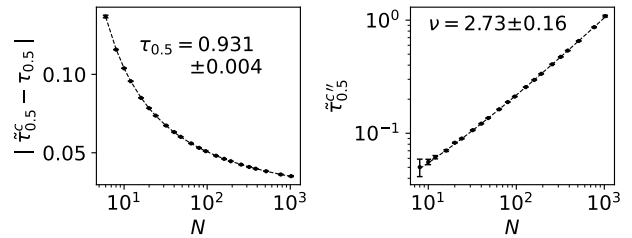

FIG. 3. Critical exponents of the topological phase transition. left: Using the fit function Eq. (F2), the effective dimension $\tilde{\tau}_q^c$, extracted from the maxima of the curves in Fig. 2 converges as a function of the system size N to $\tau_q = 0.931 \pm 0.004$. (right) system size scaling of the curvature $\tilde{\tau}_q^{c\prime\prime}$ of the fitted curves at the maxima in Fig. 2 fitted by Eq. (F3). The localisation length exponent is estimated to be $\nu = 2.73 \pm 0.16$. The irrelevant exponents are shown in App. F.

1. Disorder average and stationary phase analysis

Our starting point is the Gaussian integral

$$Z = \int D\psi\, e^{-i\bar{\psi}(E + i\delta\tau_3 - H - V)\psi}, \qquad (8)$$

where $\psi = \{\psi^a(x)\}$, $a = (s, r)$ is a $2R$ component Grassmann field, where $s = \pm$ distinguishes between retarded and advanced Green functions (corresponding to the Pauli structure $i\delta\tau_3$), and $r = 1, \dots R$ is a replica index. The Hamiltonian, H, represents the two-band model Eq. (1), and $V = V(x)\sigma_0$ is potential disorder, where σ_0 is the unit matrix, and $\langle V(x)V(x')\rangle \equiv \frac{W^2}{2}\delta(x - x')$ Gaussian correlated with zero mean.

From this functional, observables such as transport coefficients can be represented as Gaussian integrals via the introduction of suitable source terms (with an implied replica limit $R \to 0$). However, for our purposes, it will be sufficient to consider the functional as it is. Following standard protocol, we average the functional over disorder, to obtain a quartic term $\frac{W^2}{4}(\bar{\psi}\psi)^2$ in the action. Decoupling the latter by a Hubbard-Stratonovich transformation and integration over the fermion field leads a functional $Z = \int DA \exp(-S[A])$ with action $\frac{1}{W^2}\int dx\, \text{tr} A^2 - \text{tr}\ln(E + i\delta\tau_3 - H - A)$, where $A = \{A(x)^{ab}\}$ is a matrix field [27–29]. A variation of the action in this field, leads to the stationary phase equation $A(x) = \frac{W^2}{2}\text{tr}(E + i\delta\tau_3 - H - A)^{-1}(x, x)$, i.e. a self consistent Born equation with 'impurity self energy', A. We parameterize a matrix-diagonal solution compatible with the symmetry of the causal increment $i\delta\tau_3$ as $A \to \Delta E + i\kappa\tau_3$. Here, ΔE and κ are the quasiparticle energy shift and pole broadening induced by scattering, respectively. Referring for a detailed discussion of these parameters to Appendix A. We note that for infinitesimal δ, the equation admits a continuous manifold of solutions, $A = \Delta E + i\kappa Q$, where $Q = T\tau_3 T^{-1}$ with unitary $T \in \text{U}(2R)$ parameterizing the coset space mentioned in

the previous section.

Substituting these configurations into the action, and upgrading the constant T to a slowly varying Goldstone mode $T(x)$, we are led to consider the effective action

$$S[T] = -\text{tr}\ln\left(\sum_\mu v_\mu(k)\sigma_\mu + i\kappa T(x)\tau_3 T^{-1}(x)\right), \quad (9)$$

where we absorbed the energy shift ΔE into E, neglected the infinitesimal δ in comparison to κ, and introduced the four component vector v_μ with $v_0 = E$, and $v_a = -h_a$, $a = 1, 2, 3$. In the following we expand this action in slow T-fluctuations, first leaving the detailed form of the momentum-dependent coefficients $h_a = h_a(k)$ unspecified.

A. Gradient expansion

We begin our analysis of the fluctuation action with a unitary rotation of the tr ln, leading to

$$S[T] = -\text{tr}\ln\left(v_\mu\sigma_\mu + i\kappa\tau_3 + [T^{-1}, v_\mu\sigma_\mu]T)\right), \quad (10)$$

where a summation convention is applied, and the argument-dependence $v_\mu = v_\mu(k)$ and $T = T(x)$ is left implicit. Previous work performed this analysis for an effective Dirac Hamiltonian, $v_\mu = (E, -k_1, -k_2, m)$, for which the transformation of the logarithm is not innocent: It generates the chiral anomaly, and the need for UV regularization. Here, we need not worry, as we are working with a manifestly UV regular theory.

Assuming variation of the fields T over scales much larger than the lattice spacing, we approximate the commutator up to second order in derivatives as

$$[T^{-1}, v_\mu\sigma_\mu]T \simeq F_i\Phi_i - \tfrac{1}{2}J_{ij}\Phi_i\Phi_j,$$

with $F_i = i\partial_i v_\mu\sigma_\mu$, $J_{ij} = \partial_i\partial_j v_\mu\sigma_\mu$, $\Phi_i = (\partial_i T^{-1})T$, and the abbreviated notation $\partial_i v = \partial_{k_i}v$ and $\partial_i T = \partial_{x_i}T$. Our task now is to evaluate the formal second order expansion

$$S[Q] = -\text{tr}\ln\left(v_\mu\sigma_\mu + i\kappa\tau_3 + F_i\Phi_i - \frac{1}{2}J_{ij}\Phi_i\Phi_j\right) \quad (11)$$

$$= -\underbrace{\text{tr}(GF_i\Phi_i - \frac{1}{2}GJ_{ij}\Phi_i\Phi_j)}_{S^{(1)}} + \underbrace{\frac{1}{2}\text{Tr}(GF_i\Phi_i)^2}_{S^{(2)}},$$

with the Green function

$$G = (i\kappa\tau_3 + v_\mu\sigma_\mu)^{-1} = D(i\kappa\tau_3 + v_\mu\sigma^\mu),$$
$$D = [(i\kappa\tau_3 + E)^2 - h_a h_a]^{-1}, \quad (12)$$

and the convention $x_\mu y^\mu = x_0 y_0 - x_a y_a$. In the following, we discuss how the two terms above yield the sum of a gradient term, and a topological term for the effective action of the system. Both contributions are of second order in derivatives, the difference being is that one contains $\partial_i\partial_i$ derivative combinations, the other $\epsilon_{ij}\partial_i\partial_j$.

B. Topological action

In the construction of the topological action, we go fishing for antisymmetric derivative combinations $\epsilon_{ij}\partial_i\partial_j$. As we show in Appendix B these emerge from both terms $S^{(1)}$ and $S^{(2)}$. On this basis, we obtain the topological action

$$S_{\text{top}} = S_{\text{top}}^{(1)} + S_{\text{top}}^{(2)} = \frac{\theta_2 + \theta_1}{16\pi}\int dx\,\mathcal{L}_{\text{top}}(Q),$$
$$\mathcal{L}_{\text{top}}(Q) \equiv \epsilon_{ij}\,\text{tr}(Q\partial_i Q\partial_j Q), \quad (13)$$

with coupling constants

$$\theta_1 = 8\kappa\int(dk)D^+ D^- F_k,$$

$$\theta_2 = 4\pi i\int(dk)\int_E^\infty d\omega\,(D_\omega^{+2} - D_\omega^{-2})F_k \quad (14)$$

where $(dk) = \frac{dk_1 dk_2}{(2\pi)^2}$ and

$$F_k = \epsilon_{abc}h_a\partial_1 h_b\partial_2 h_c = (\partial_1 h \times \partial_2 h)\cdot h. \quad (15)$$

(Following standard conventions [10, 17]), we associate the one/two derivative action $S^{(1/2)}$ with the two/one contribution to the topological action, $\theta_{2/1}$.) Our final task thus is to compute the coefficients $\theta_{1,2}$. These integrals are straightforward for weak disorder, under a presumed hierarchy of energy scales

$$\kappa \ll E \lesssim 1. \quad (16)$$

We first represent the propagators D^s as

$$D^s = \frac{1}{E^2 - \epsilon^2 + is\gamma\tau_3}, \qquad \gamma = 2\kappa E, \quad \epsilon^2 = \sum_a h_a^2.$$

Under the stated conditions, this leads to the approximation

$$\kappa D^+ D^- = \frac{\kappa}{(E^2 - \epsilon^2)^2 + \gamma^2} \simeq \frac{\pi}{4E^2}\delta(E - \epsilon), \quad (17)$$

where here and throughout, $\epsilon > 0$ is the positive root of ϵ^2. Thus,

$$\theta_1 \simeq \frac{2\pi^2}{E^2}\int(dk)F_k\delta(E - \epsilon),$$

which is an on-shell integral probing the density of states at E. Turning to θ_2, we note $D_\omega^{s2} \simeq \partial_{\omega^2}D_\omega^s$, and

$$D_\omega^+ - D_\omega^- \simeq -\frac{\pi i}{\omega}\delta(\omega - \epsilon)$$

Entering with these relations into the integral defining θ_1 and integrating by parts, it is straightforward to verify that

$$\theta_2 \simeq 2\pi^2\int(dk)F_k\left(\frac{\Theta(\epsilon - E)}{\epsilon^3} - \frac{\delta(\epsilon - E)}{\epsilon^2}\right).$$

We note that the second, on-shell term cancels against θ_1. To understand the meaning of the first, recall that $\epsilon = |h|$. We may thus define the unit sphere area element $S \equiv F/\epsilon^3 = n\cdot(\partial_1 n \times \partial_2 n)$ with unit vector $n = h/\epsilon$. Tidying up, we obtain the topological angle as in Eq. (3).

C. Gradient action

The gradient term of the action is obtained by similar inspection of $S^{(1,2)}$, this time focusing on derivative combinations of the form $\sim F_i F_i$. As detailed in Appendix C, this leads to

$$S_{\text{grad}} = I \int dx \, \text{tr} \left(\partial_i Q \partial_i Q \right),$$
$$I = I_+ + I_- + I_{+-}, \qquad (18)$$

with coupling constants given by

$$I_{+-} = \frac{1}{2} \sum_a \int (dk)(E^2 + \kappa^2 - \epsilon^2 + 2h_a^2) D^+ D^- \partial_i h_a \partial_i h_a,$$

$$I_{\pm} = \frac{1}{4} \sum_a \int (dk)((E + i \pm \kappa)^2 - \epsilon^2 + 2h_a^2) D^{\pm 2} \, \partial_i h_a \partial_i h_a.$$
$$(19)$$

We are left with the task to do the momentum integrals. For weak disorder, these integrals are analytically doable, if somewhat tedious. As a result, detailed in Appendix D, we obtain

$$I = \frac{E^2 - m^2}{2|E|\kappa} \Theta(E^2 - m^2), \qquad (20)$$

where $m = (r - c)$ and $c = 2, 0, -2$ depending on the Dirac cone around which we approximate.

This result states that for weak disorder, diffusive quasiparticle propagation is limited to energies above the clean insulator band gap, m. For energies $E \gg m$, the coupling constant asymptotes to $\sim E/\kappa$ which is the characteristic scale for the conductivity of a weakly disordered two-dimensional conductor.

D. Beyond the weak disorder limit

From Eq.(14) we may calculate angle θ for arbitrary two-band Hamiltonians H and for values (r, E, W) such that the self consistent Born approximation underlying our theory remains valid, $E\kappa \gtrsim 1$. However, outside the weak disorder regime $E\kappa \gg 1$ considered in the previous section the analytical computation of the integrals becomes cumbersome, or even impossible.

Progress can nevertheless be made, starting from the following representation of the coupling constants in terms of energy/momentum integrals:

$$\theta_1 = -\frac{i\pi}{2} \int (dk) \, \epsilon_{ij} \, \text{tr} \left(\tau_2 G_E \partial_i G_E^{-1} \tau_1 G_E \partial_j G_E^{-1} \right),$$

$$\theta_2 = \frac{\pi \epsilon_{\alpha\beta\gamma}}{3} \int_{-\infty}^{E} d\omega \int (dk) \times \qquad (21)$$
$$\times \, \text{tr} \left(\tau_3 G_\omega \partial_\alpha G_\omega^{-1} G_\omega \partial_\beta G_\omega^{-1} G_\omega \partial_\gamma G_\omega^{-1} \right),$$

where $G = G_E$ is the SCBA Green function Eq.(12), latin indices take the values $i, j = 1, 2$ and the Greek indices

the values $\alpha, \beta, \gamma = \omega, 1, 2$. Referring for the derivation of these representations from Eq.(14) to Appendix E, we note that in the IQH context these integral representations are known as the Smrcka-Streda [17] Hall coefficients, $\sigma_{xy}^{\text{I}} = \theta_1/2\pi$, and $\sigma_{xy}^{\text{II}} = \theta_2/2\pi$. These parameters describe the Fermi surface (σ_{xy}^{I}) and thermodynamic (σ_{xy}^{II}, note the integral over all energies below the Fermi surface) contribution to the Hall response $\sigma_{xy} = \sigma_{xy}^{\text{I}} + \sigma_{xy}^{\text{II}}$ of an electron gas subject to a magnetic field.

We may now numerically compute the complex self energy $\Delta E + i\kappa$ in self-consistent Born approximation along the lines of section III 1, and then do the integrals. This procedure yields estimates for the topological angle, which however remain of limited accuracy. Deviations arise because of the reliance on the SCBA, whose range of applicability is limited to $E \gg \kappa$ and $\sigma_{xx} \gg 1$. For the former condition, if we go outside this regime, the self energy κ is affected by scattering processes technically described by diagrams with crossing impurity scattering and for the latter condition $\sigma_{xx} \sim \mathcal{O}(1)$ indicates close proximity to the quantum Hall critical point, where the approach discussed in this paper is no longer suitable. While we did not investigate the contributions from further scattering processes in quantitative detail, our comparison to exact diagonalization shows that we obtain reasonable agreement, including in regimes where the theory is past the region of parametric control.

IV. COMPARISON TO EXACT DIAGONALIZATION

In figure 4 we compare the results obtained from numerical simulations (section II C) with the analytical predictions (section III) for the position of the extended state in the band of eigenstates. Numerically, we identify these states by calculation of the exponent $\tau_q = 2(1-q) + \Delta_q$, at quantum Hall criticality, $\Delta_q = 0.25 \times q(q-1)$, for the extremal value $q = 0.5$, i.e. $\Delta_{\min} = \Delta_{q=0.5} \approx -0.06$, and $\tau_{0.5} \approx 0.94$. The leftmost panel shows the system size dependent $\tau_{0.5}^N$ for $r = 1.2$, $W = 1.45$ as a function of E. At the above value $\tau_{0.5}^N \approx \tau_{0.5} \approx 0.94$ (green arrow) the data becomes system size independent, signifying criticality with an exponent matching the quantum Hall expectation.

To compare to the field theory predictions, we compute σ_{xy} by numerical evaluation of Eqs. (21) for the same values of r and W (blue curve). The crossing of the critical conductance $\sigma_{xy} = \frac{1}{2}$ is indicated by a blue arrow. The analytical and numerical predictions are not in perfect, but in reasonable agreement, given that there are no adjustable fitting parameters.

The center panel shows the energy of the extended state at $r = 1.7$ (left) and $r = 1.2$ (right) as a function of the disorder strength W. The green curves show the analytically computed longitudinal conductance, where $\sigma_{xx} \gtrsim 1$ is necessary for quantiative reliability of the field theory. As long as this condition is met, the analyt-
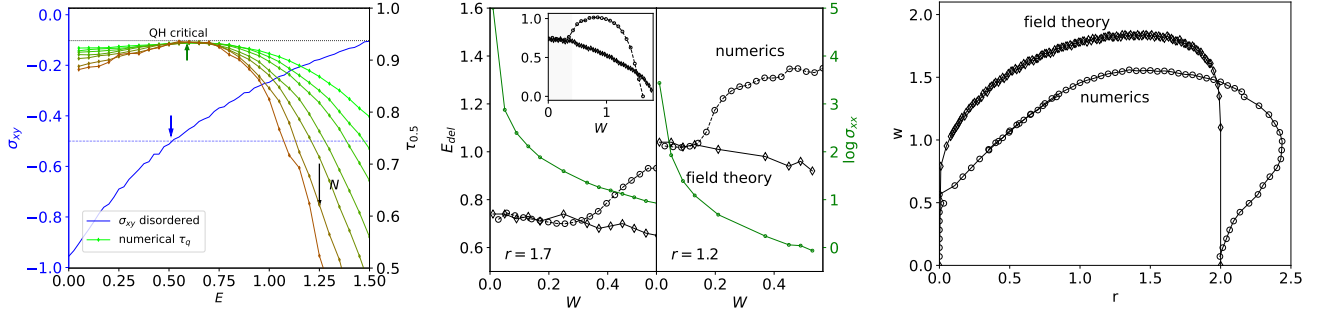
FIG. 4. Analytical and numerical prediction for the position of the extended state. Left: the blue solid line shows the Hall conductivity calculated from Eq. (3), for different energies, at $(r, W) = (1.2, 1.45)$, while the blue dashed line shows the Hall conductivity for the clean Chern insulator at $r = 1.2$. Criticality is associated with the value $\sigma_{xy}(E) = 1/2 \bmod 1$, cf. blue arrow. On the right axis the numerical results for the effective dimensions $\tau_q(E)$ [30] for different system sizes $N = 64$ (green) up to $N = 512$ (red) are shown (black arrow). The dotted horizontal line is the dimension $\tau_{0.5} \approx 0.94$ of the quantum Hall critical state. This condition is approximately met at the green arrow, which is reasonably, but not perfectly well aligned with the blue analytical marker. Center: prediction for the delocalized states taken from multifractal analysis and field theory at $r = 1.7$ and $r = 1.2$ as a function of disorder strength W. Additionally the analytically calculated σ_{xx} is shown (green). The inset shows the behavior of the delocalized state calculated with both analytical and numerical approaches for the full topological phase at $r = 1.7$. Right: phase diagram of the disordered Chern insulator in the r-W-plane at $E = 0$, calculated analytically and numerically.

ical and numerical predictions for the value of the critical energy are in good agreement. At larger values of the disorder, σ_{xy} is at its critical value, and $\sigma_{xx} = \mathcal{O}(1)$, so we are in proximity to the quantum critical point where the present theory is no longer applicable. In this regime, the numerical prediction for the critical energy shows a transient increase (cf. inset) for which we do not have a good explanation. Eventually, the numerical and analytical value for the critical energy approach zero — that they do so at roughly the same disorder concentration may be coincidental — thus signalling the breakdown of the topological phase due to disorder.

The right panel shows a cut through the critical surface at $E = 0$. Inside the lobe we have the Chern number $\mathrm{Ch}_c = -1$, outside it is vanishing. Broadly speaking, we again observe semi-quantitative parameter free agreement between field theory and numerics. However, there are some qualitative features which the former does not capture: Close to the clean critical value, $r = 2$, disorder stabilizes the topological phase in that the critical value gets pushed upwards (the bulge visible in the numerical data.) This feature does not show in the field theoretical calculation. We suspect that this is due to the fact that we are in parametric proximity to a Dirac band closing at weak disorder and zero energy. For such configurations, the SCBA approximation produces incorrect estimates for self energies[31]. However, a more detailed analysis of the latter beyond the SCBA approximation is beyond the scope of the present paper.

V. CONCLUSIONS

In the disordered Chern insulator, the spectral gap of the clean insulator is replaced by a mobility gap: generic states inside the spectrum are Anderson localized, thus preventing bulk hybridization between the extended surface states of the system. However, this feature cannot extend to all states: there must exist bulk delocalized states establishing contact between the surface bands somewhere up in the spectrum. However, these consistency arguments do not tell us where the delocalized states lie in energy, nor what their critical properties are. The study of these two questions was the subject of the present paper.

Describing the Chern insulator in terms of the three parameters band energy, E, effective disorder strength, W, and a parameter, r, controlling its topological index $\nu(r)$, we applied a combination of analytical and numerical methods to study the 'critical surface' of delocalized states in the Chern insulator. For generic parameter values, the critical states are buried deep in the band, meaning that these analyses had to operate outside the regime where 'Dirac' band linearlizations are an option. Perhaps unexpectedly, this generalization turned out to be a blessing, from various perspectives: The analytical derivation of an effective field theory building on the full microscopic band structure was no more difficult than the one starting from a linearized spectrum. However, unlike that one, it was not plagued by spurious ultraviolet divergences, and it produced intuitive predictions for the identification of the critical states. Specifically, we found that, at least for weak disorder, criticality was tied to the integral Eq.(3): the energy of critical states in the weakly disordered system is such that the inte-

grated Berry curvature of a all states above (or below) it equals π. The effective action describing the localization properties of these and of generic states was that of the quantum Hall insultator, confirming the expectation of bulk quantum Hall crticality in the system. However, for generic points in the parameter space (r, W, E) the weak disorder condition required for this description to be quantitatively reliable was violated, and quantitative errors ahad to be expected.

To benchmark the quality of the analytical predictions, we analyzed the eigenstates of the system by numerical methods. Specifically, we computed the wave function scaling dimensions τ_q, Eqs. (4), (5) to identify both the position of the extended states in parameter space, and their critical properties. This analysis confirmed the expectation of quantum Hall criticality, and for sufficiently weak disorder the results obtain by the field theoretical computation. Outside that regime, the quality of the analytical predictions deteriorated, with errors up to $\mathcal{O}(1)$, but no parametric disagreement.

The Chern insulator is one of the simplest topological insulators, and features as an effective building block for others. In view of the fact, that even basic signatures of the (surface) criticality of disordered topological insulators remain mysterious[32], it is reassuring to have this basic system under control. We hope that the insights gained here may help in the solution of the more challenging problem of understanding the surface criticality of disordered three-dimensional topological insulators.

VI. ACKNOWLEDGMENTS

Appendix A: Self consistent Born approximation

In this appendix we discuss more in depth the self consistent Born approximation and in general the role of the parameters κ and ΔE. The starting point is the self consistent Born equation for the matrix $A(x)$,

$$A(x) = W^2 \operatorname{tr} \left(E + i\delta\tau_3 - H - A \right)^{-1} (x, x).$$

We propose a spatially homogeneous and matrix diagonal Ansatz of the form $\bar{A} = \Delta E + i\kappa\tau_3$. Plugging in the Ansatz into the previous expression, we obtain a self-consistent equation for both ΔE and κ.

$$\Delta E + i\kappa\tau_3 = \frac{W^2}{2} \int_{BZ} \frac{d^2 k}{(2\pi)^2} \operatorname{tr} \left(\frac{1}{E - H(k) - \Delta E - i\kappa\tau_3} \right).$$

The real part of the previous equation, ΔE, represents nothing more than an overall shift in the energy E of the system. The imaginary part is the self energy due to impurity scattering which is to be identified with (2 times) the scattering rate off impurities and consequently defines another quantities of interest such as the elastic scattering time τ and the mean free path ℓ.

Appendix B: Derivation of the topological action

We here derive Eq.(13) for the topological action by explicit computation of the two contributing terms $S_{\text{top}}^{(1,2)}$, i.e. the skew-derivative contributions to the first and second order gradient term in Eq. (11).
$S_{\text{top}}^{(2)}$: The expanded representation of the second order term reads

$$
\begin{aligned}
S^{(2)}[Q] &= \frac{1}{2} \int dx (dk) \operatorname{tr}(D(i\kappa\tau_3 + v_\mu\sigma^\mu) F_i \Phi_i D(i\kappa\tau_3 + v_\nu\sigma^\nu) F_{\bar{i}} \Phi_{\bar{i}}) \\
&\rightarrow -\frac{1}{2} \int dx (dk) \operatorname{tr}(D(i\kappa\tau_3 + v_\mu\sigma^\mu)(\sigma_a \partial_i h_a \Phi_i) D(i\kappa\tau_3 + v_\nu\sigma^\nu)(\sigma_b \partial_{\bar{i}} h_b \Phi_{\bar{i}})) \\
&= -i\kappa \int dx (dk) \operatorname{tr}(D\tau_3(\sigma_a \partial_i h_a \Phi_i) D(h_c \sigma_c)(\sigma_b \partial_{\bar{i}} h_b \Phi_{\bar{i}})) \\
&= -2\kappa\epsilon_{abc} \int dx (dk) \operatorname{tr}(D\tau_3 \Phi_i D\Phi_{\bar{i}}) \partial_i h_a \partial_{\bar{i}} h_b h_c = -2\kappa\epsilon_{ij} \int dx (dk) \operatorname{tr}(D\tau_3 \Phi_i D\Phi_j) F_k, \quad \text{(B1)}
\end{aligned}
$$

where $(dk) = dk_1 dk_2 / (2\pi)^2$, the arrow indicates that we retain only derivative combinations $\partial_i \partial_{\bar{i}}$, $\bar{i} = (i+1) \bmod 2$, and we used the definition Eq. (15). To process the integral over k, we decompose the matrices $D = D^+ P^+ + D^- P^-$, $P^s = \frac{1}{2}(1 + s\tau_3)$ into advanced and retarded contributions and note that only momentum integrals

over denominators $D^+ D^-$ of opposite causality are non-vanishing. In this way we arrive at

$$S_{\text{top}}^{(2)}[Q] = -\frac{\theta_1}{4\pi} \int dx \sum_s s\epsilon_{ij} \, \text{tr}(P^s \Phi_i P^{\bar{s}} \Phi_j), \quad (B2)$$

with the momentum integral θ_2 defined in Eq. (14). We finally use the first of the auxiliary relations

$$-4\epsilon_{ij} \sum_s \text{tr}(sP^s \Phi_i P^{\bar{s}} \Phi_j) = \mathcal{L}_{\text{top}}(Q),$$

$$4\epsilon_{ij} \text{tr}(\tau_3 \partial_i \Phi_j) = \mathcal{L}_{\text{top}}(Q), \quad (B3)$$

to obtain $S_{\text{top}}^{(2)}$ as given in Eq. (13).

$S_{\text{top}}^{(2)}$: Being first order in derivatives, the contribution from the term $S^{(1)}$ naively seems to vanish. To see that it does not, we play a trick first applied by Pruisken in his analysis of the quantum Hall effect. Noting that the energy-dependent Green function $G \equiv G_E$ can be written as $G_E = \int_E^\infty d\omega \, G_\omega^2$, we represent the action as (in the same notation, $D_\omega \equiv D_{E=\omega}$)

$$S_{\text{top}}^{(1)}[Q] = -\int_E^\infty d\omega \, \text{Tr}(G_\omega F_i \Phi_i G_\omega) \rightarrow -\frac{i}{2} \int_E^\infty d\omega \int dx(dk) \, \text{tr}((\partial_j G_\omega)F_i(\partial_j \Phi_i)G_\omega - G_\omega F_i(\partial_j \Phi_i)\partial_j G_\omega)$$

$$= -\frac{i}{2} \int_E^\infty d\omega \int dx(dk) \, \text{tr}([(\partial_j G_\omega), G_\omega]F_i \partial_j \Phi_i) = -\frac{1}{2} \int_E^\infty d\omega \int dx(dk) \, \text{tr}(D_\omega^2 [\partial_j(h_a \sigma_a), h_b \sigma_b](\partial_i h_c \sigma_c)\partial_j \Phi_i)$$

$$= -2i \int_E^\infty d\omega \int dx(dk)\epsilon_{ij} \, \text{tr}(D_\omega^2 \partial_j \Phi_i)F_k. \quad (B4)$$

We now decompose the matrix D again, and note that only the contribution proportional to τ_3 yields a non-vanishing trace, $D^2 \rightarrow \frac{1}{2}(D^{+2} - D^{-2})\tau_3$. As a result, we obtain

$$S_{\text{top}}^{(1)}[Q] = \frac{\theta_2}{4\pi} \int dx \, \epsilon_{ij} \, \text{tr}(\tau_3 \partial_i \Phi_j), \quad (B5)$$

with θ_2 given in (14). In a final step, we use the second of the auxiliary relations (B3) to arrive at the contribution

$S^{(1)}$ to (13).

Appendix C: Derivation of the gradient action

We here derive Eq. (18) by inspection of the two terms $S^{(1,2)}$ in the formal gradient expansion Eq. (11).

$S_{\text{grad}}^{(1)}$: Filtering symmetric derivative combinations from the explicit representation of the second order expansion we obtain

$$S_{\text{grad}}^{(2)}[Q] = \frac{1}{2} \int dx(dk) \, \text{tr}(D(i\kappa\tau_3 + v_\mu \sigma^\mu)F_i \Phi_i D(i\kappa\tau_3 + v_\nu \sigma^\nu)F_j \Phi_j)$$

$$\rightarrow -\frac{1}{2} \int dx \, (dk) \, \text{tr}\left(-\kappa^2 D\tau_3 \sigma_\nu \Phi_i D\tau_3 \sigma_\lambda \Phi_i + Dv_\mu \sigma^\mu \sigma_\nu \Phi_i Dv_\rho \sigma^\rho \sigma_\lambda \Phi_i + 2iE\kappa \, D\tau_3 \sigma_\nu \Phi_i D\sigma_\lambda \Phi_i\right) \partial_i v_\nu \partial_i v_\lambda$$

$$= -\int dx(dk) \sum_a \text{tr}\left(-\kappa^2 \, \tau_3 D\Phi_i \tau_3 D\Phi_i + (E^2 - \epsilon^2 + 2h_a^2)D\Phi_i D\Phi_i + 2iE\kappa \, D\tau_3 \Phi_i D\Phi_i\right) \partial_i h_a \partial_i h_a,$$

where "$\rightarrow$" indicates that we retain only derivatives with identical i-index, and in the second equality traced over Pauli matrices. To compute the k-integrals, we again decompose $D = D^+ P^+ + D^- P^-$. The product of two D's then leads to terms $D^s D^{s'}$ of equal and opposite causal index s, s', which need to be considered separately.

Using the auxiliary relations

$$\sum_s \text{tr}\left(\Phi_i \tau_3^n P^s \Phi_i \tau_3^m P^{-s}\right) = \frac{1}{4} \text{tr}\left(\partial_i Q \partial_i Q\right) \times$$

$$\times \begin{cases} -1 & (n,m) = (0,0), \\ 1 & (n,m) = (1,1), \\ 0 & (n,m) = (0,1), (1,0) \end{cases},$$

and

$$\sum_s \text{tr}\left(\Phi_i \tau_3^n P^s \Phi_i \tau_3^m P^s\right) f_s =$$

$$= -\sum_s s^{n+m} \text{tr}\left(\frac{1}{4}\partial_i Q \partial_i Q - P^s \Phi_i^2\right) f_s,$$

where f_s is arbitrary, it is straightforward to obtain

$$S_{\text{grad}}^{(2)}[Q] = (I_+ + I_- + I_{+-})\int dx\, \text{tr}\left(\partial_i Q \partial_i Q\right) + S_A,$$

(C1)

with $S_A = 4\sum_s I_s \int dx\, \text{tr}(P^s \Phi_i^2)$, and the coefficients defined in Eq. (19)

$S_{\text{grad}}^{(1)}$: The terms with equal indices, J_{ii} in Eq. (11) yield

a term

$$S_{\text{grad}}^{(1)} = \frac{1}{2}\text{Tr}(G J_{ii}\Phi_i^2),$$

$$= \frac{1}{2}\int dx(dk)\sum_s \text{tr}\left(G^s P^s \partial_i^2 v_\mu \sigma_\mu \Phi_i^2\right),$$

$$= \frac{1}{2}\int dx(dk)\sum_s \text{tr}\left(G^s \partial_i v_\nu \sigma_\nu G^s \partial_i v_\mu \sigma_\mu P^s \Phi_i^2\right),$$

$$= -S_A$$

where we integrated by parts and used that $\partial_i G^s = -G^s \partial_i h_\nu \sigma_\nu G^s$. We conclude that the anomalous terms, S_A cancel out and arrive at the full gradient action Eq. (18).

Appendix D: Derivation of Eq. (20)

In this appendix we take a closer look at the derivation of equation (20). The first thing to notice is that I can be written as the following,

$$I = \frac{1}{4}\sum_a \int (dk)((E+i\kappa)D^+ + (E-i\kappa)D^-)^2 + (2h_a^2 - \epsilon^2)(D^+ + D^-)^2(\partial_i h_a \partial_i h_a),$$

$$= \sum_a \int (dk)\frac{E^2(E^2 + \kappa^2 - \epsilon^2)^2 + (2h_a^2 - \epsilon^2)(E^2 - \kappa^2 - \epsilon^2)^2}{((E^2 - \kappa^2 - \epsilon^2)^2 + 4E^2\kappa^2)^2}(\partial_i h_a \partial_i h_a),$$

$$= \sum_a \int (dk)\frac{E^2(E^2 + \kappa^2 - \epsilon^2)^2 + (2h_a^2 - \epsilon^2)(E^2 - \kappa^2 - \epsilon^2)^2}{((E^2 - \kappa^2 - \epsilon^2)^2 + 4E^2\kappa^2)(2|E|\kappa)}\left(\frac{2|E|\kappa}{(E^2 - \kappa^2 - \epsilon^2)^2 + 4E^2\kappa^2}\right)(\partial_i h_a \partial_i h_a).$$

To make further progress we take the limit when $E\kappa \to 0$ resulting in,

$$I = \pi \sum_a \int (dk)\frac{E^2 - \epsilon^2 + 2h_a^2}{2|E|\kappa}(\partial_i h_a \partial_i h_a)\delta(E^2 - \epsilon^2),$$

$$= \pi \int (dk)\frac{\sum_a h_a^2(\partial_i h_a \partial_i h_a)}{|E|\kappa}\delta(E^2 - \epsilon^2).$$

At this point we focus in the low energy regime, where we can take the Dirac approximation, resulting in,

$$I = \frac{E^2 - m^2}{2|E|\kappa}\Theta(E^2 - m^2),$$

with $m = r - c$ and $c = 2, 0, -2$ depending on the Dirac cone around which we approximate.

Appendix E: Derivation of the Smrcka-Streda coefficients

In this appendix we show the relation between the equations 14 and the equations (21). More precisely, we want to show that $\theta_1 = 2\pi\sigma_{xy}^I$ and $\theta_2 = 2\pi\sigma_{xy}^{II}$.

$$\sigma_{xy}^I = -\frac{i}{16\pi^2} \int dk\, \epsilon_{ij}\, \mathrm{tr}\left(\tau_2 G_E \partial_i G_E^{-1} \tau_1 G_E \partial_j G_E^{-1}\right),$$

$$= \frac{1}{8\pi^2} \sum_s \int dk\, s\, \mathrm{tr}((G_E \partial_1 G_E^{-1})_s (G_E \partial_1 G_E^{-1})_{-s}),$$

$$= \frac{1}{8\pi^2} \sum_s \int dk\, s\, \mathrm{tr}\left((E + is\kappa + h_a\sigma_a)(\partial_1 h_b\sigma_b)(E - is\kappa + h_c\sigma_c)(\partial_2 h_d\sigma_d)\right) D^s D^{-s},$$

$$= -\frac{i\kappa}{2\pi^2} \int dk\, \mathrm{tr}(\sigma_a\sigma_b\sigma_c) h_a \partial_1 h_b \partial_2 h_c D^+ D^-,$$

$$= \frac{\kappa}{\pi^2} \int dk\, D^+ D^- F_k,$$

$$= \theta_1/(2\pi),$$

$$\sigma_{xy}^{II} = \frac{1}{24\pi^2} \int_{-\infty}^{E} \int d\omega dk\, \epsilon_{\alpha\beta\gamma}\, \mathrm{tr}\left(\tau_3 G_\omega \partial_\alpha G_\omega^{-1} G_\omega \partial_\beta G_\omega^{-1} G_\omega \partial_\gamma G_\omega^{-1}\right), \tag{E1}$$

$$= \frac{1}{8\pi^2} \sum_s \int_{-\infty}^{E} d\omega \int dk\, s\, \mathrm{tr}\left(((G_\omega \partial_1 G_\omega^{-1})_s (G_\omega \partial_2 G_\omega^{-1}) - (G_\omega \partial_1 G_\omega^{-1})_s (G_\omega \partial_2 G_\omega^{-1}) G_\omega)\right),$$

$$= \frac{1}{8\pi^2} \sum_s \int_{-\infty}^{E} d\omega \int dk\, s\, \mathrm{tr}\left([(\partial_1 G_\omega)_s, (G_\omega)_s] \partial_2 (G_\omega^{-1})_s\right),$$

$$= \frac{1}{8\pi^2} \sum_s \int_{-\infty}^{E} d\omega \int dk\, s\, \mathrm{tr}\left([(\omega + is\kappa + h_a\sigma_a), \partial_1 h_b\sigma_b] \partial_2 h_c\sigma_c\right) D_s^2,$$

$$= \frac{1}{4\pi^2} \int_{-\infty}^{E} d\omega \int dk\, \mathrm{tr}(\sigma_a\sigma_b\sigma_c) h_a \partial_1 h_b \partial_2 h_c (D_+^2 - D_-^2),$$

$$= \frac{i}{2\pi^2} \int_{-\infty}^{E} d\omega \int dk\, F_k((D_+^2 - D_-^2)),$$

$$= \theta_2/(2\pi).$$

Appendix F: Details of the multifractal analysis

This section provides supportive data to show that the critical lines shown in Fig. 4 can be identified with quantum Hall criticality.

1. Distribution functions of the moments

Fig. 5 shows the distribution functions for the critical point associated with the delocalised state found analytically in Fig. 4 (left). The shape of the distribution function as well as their mean converge to a power law scaling governed by the effective dimension of the quantum Hall effect, known from other numerical works. [22] This can be most convincingly seen in the collapsed curves in the inset of Fig. 5.

2. Extrapolation of the critical exponents

In order to find the critical point at which we can compare to quantum Hall criticality in the first place we cal-

culate $\tilde{\tau}_q(E, W, r)$ at $q = 0.5$ as described in the main text for all available system sizes, and find their local maxima.

A cut through phase space close to the critical point $(E^*, W^*, r^*) \approx (0.6, 1.45, 1.2)$ is shown in Fig. 2.

The extrapolation of the critical properties is done by fitting the curves using the model

$$\tilde{\tau}_q = \tilde{\tau}_q^c + \frac{1}{2}\tilde{\tau}_q^{c\,\prime\prime}(W - W^c)^2 + \beta^c(W - W^c)^3, \tag{F1}$$

where the superscript c denotes the fitted values at criticality for a given system size N, and α^c the opening angle of the parabolic part of the curve, from which the curvature, and the localization length exponent can be extracted. We use a third order model to account for asymmetries in the curves.

In Fig. 3 we present a more detailed analysis of the system size scaling of the data for the effective dimension in Fig. 2. Since we approximate the true effective dimension τ_q by the maxima of $\tilde{\tau}_q$, we need to extrapolate to $N \to \infty$. This is done by the fitting function

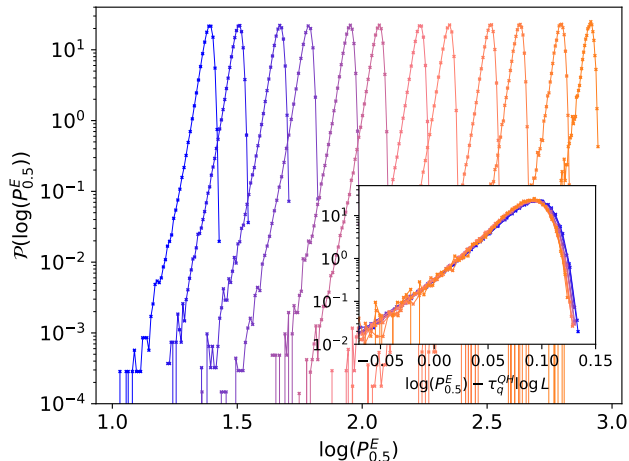$$\tilde{\tau}_q^c(N) = \tau_q + \frac{a}{\log N} + b\, N^{-y_\tau}, \tag{F2}$$

FIG. 5. Distribution functions of $P_{0.5}$ at $E = 0.59, W = 1.45, r = 1.2$. According to the field theoretical calculations a quantum Hall critical states should exist here. The distribution functions correspond to different system sizes, $L = 16, 24, 32, 48, 64, 96, 128, 192, 256, 384, 512, 768, 1024$ (blue to red). Not only their mean, which is relevant for the scaling, but the full distribution function collapses to a power law governed by the quantum Hall critical dimension $\tau_{0.5}^{QH} \approx 0.94$ (inset).
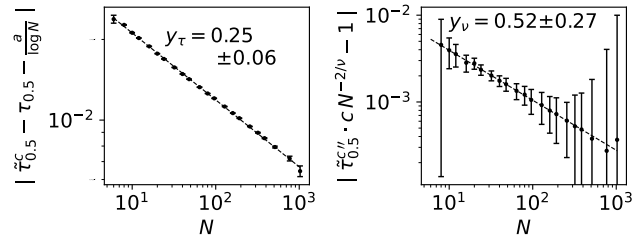

FIG. 6. (left) The irrelevant system size scaling of the fitted maxima without the logarithmic part originating from the simplified definition of $\tilde{\tau}_q$. (right) irrelevant exponent y_ν from the fitting function in Eq. (F3). The irrelevant exponents quantify the finite size corrections associated with the exponents extracted in Fig. 2.

where the fitting parameter a corresponds to the prefactor of the system size scaling of the wave function moments in Eq. (5) and y_τ approximates the exponent of an irrelevant scaling correction.

Additionally, we show the localization length exponent ν extracted from the curvature of the curves in Fig. 2. The latter is supposed to scale as

$$\tilde{\tau}_q^{c\,\prime\prime} = c\,N^{2/\nu}\left(1 + d\,N^{-y_\nu}\right), \tag{F3}$$

where again y_ν denotes the corresponding irrelevant exponent. We find $\nu = 2.73 \pm 0.16$ and $y_\nu = 0.52 \pm 0.27$ as described in the main text.

[1] F. D. M. Haldane, Model for a quantum Hall effect without landau levels: Condensed-matter realization of the "parity anomaly", Physical Review Letters **61**, 2015 (1988).

[2] J. Li, R.-L. Chu, J. K. Jain, and S.-Q. Shen, Topological Anderson insulator, Physical review letters **102**, 136806 (2009).

[3] C. Groth, M. Wimmer, A. Akhmerov, J. Tworzydło, and C. Beenakker, Theory of the topological Anderson insulator, Physical review letters **103**, 196805 (2009).

[4] R. Prange, Quantized Hall resistance and the measurement of the fine-structure constant, Physical Review B **23**, 4802 (1981).

[5] M. V. Berry, Quantal phase factors accompanying adiabatic changes, Proceedings of the Royal Society of London. A. Mathematical and Physical Sciences **392**, 45 (1984).

[6] D. J. Thouless, M. Kohmoto, M. P. Nightingale, and M. den Nijs, Quantized Hall conductance in a two-dimensional periodic potential, Physical review letters **49**, 405 (1982).

[7] B. Simon, Holonomy, the quantum adiabatic theorem, and Berry's phase, Physical Review Letters **51**, 2167 (1983).

[8] C. L. Kane and E. J. Mele, Quantum spin Hall effect in graphene, Physical review letters **95**, 226801 (2005).

[9] E. Abrahams, P. Anderson, D. Licciardello, and T. Ramakrishnan, Scaling theory of localization: Absence of quantum diffusion in two dimensions, Physical Review Letters **42**, 673 (1979).

[10] A. M. Pruisken, On localization in the theory of the quantized Hall effect: A two-dimensional realization of the θ-vacuum, Nuclear Physics B **235**, 277 (1984).

[11] H. Levine, S. B. Libby, and A. M. Pruisken, Theory of the quantized Hall effect (i), Nuclear Physics B **240**, 30 (1984).

[12] D. Khmelnitskii, Quantization of Hall conductivity, ZhETF Pisma Redaktsiiu **38**, 454 (1983).

[13] P. M. Ostrovsky, I. V. Gornyi, and A. D. Mirlin, Quantum criticality and minimal conductivity in graphene with long-range disorder, Phys. Rev. Lett. **98**, 256801 (2007).

[14] W. Pauli and F. Villars, On the invariant regularization in relativistic quantum theory, Rev. Mod. Phys. **21**, 434 (1949).

[15] C. G. Bollini and J. J. Giambiagi, Dimensional renormalization: The number of dimensions as a regularizing parameter, Il Nuovo Cimento B (1971-1996) **12**, 20 (1972).

[16] M. Veltman *et al.*, Regularization and renormalization of gauge fields, Nuclear Physics B **44**, 189 (1972).

[17] L. Smrcka and P. Streda, Transport coefficients in strong magnetic fields, Journal of Physics C: Solid State Physics **10**, 2153 (1977).

[18] F. Evers and A. D. Mirlin, Anderson transitions, Reviews

of Modern Physics **80**, 1355 (2008).

[19] A. Mirlin and F. Evers, Multifractality and critical fluctuations at the Anderson transition, Physical Review B **62**, 7920 (2000).

[20] A. Rodriguez, L. J. Vasquez, K. Slevin, and R. A. Römer, Multifractal finite-size scaling and universality at the Anderson transition, Physical Review B **84**, 134209 (2011).

[21] M. Puschmann, D. Hernangómez-Pérez, B. Lang, S. Bera, and F. Evers, Quartic multifractality and finite-size corrections at the spin quantum Hall transition, Physical Review B **103**, 235167 (2021).

[22] F. Evers, A. Mildenberger, and A. Mirlin, Multifractality at the quantum Hall transition: Beyond the parabolic paradigm, Physical review letters **101**, 116803 (2008).

[23] F. Evers, A. Mildenberger, and A. Mirlin, Multifractality of wave functions at the quantum hall transition revisited, Physical Review B **64**, 241303 (2001).

[24] M. Puschmann, P. Cain, M. Schreiber, and T. Vojta, Integer quantum Hall transition on a tight-binding lattice, Physical Review B **99**, 121301 (2019).

[25] M. Puschmann and T. Vojta, Green's functions on a renormalized lattice: An improved method for the integer quantum hall transition, Annals of Physics **435**, 168485 (2021).

[26] E. J. Dresselhaus, B. Sbierski, and I. A. Gruzberg, Scaling collapse of longitudinal conductance near the integer quantum Hall transition, Physical Review Letters **129**, 026801 (2022).

[27] A. Altland, C. Offer, and B. Simons, Supersymmetry and trace formulae (1999).

[28] K. Efetov, *Supersymmetry in disorder and chaos* (Cambridge University Press, 1999).

[29] A. Altland and B. D. Simons, *Condensed matter field theory* (Cambridge university press, 2010).

[30] Here for a better visualization of the convergence, of the value of the effective dimension itself we calculate $\tau_q^N = (\log(P_q^N) - \log(P_q^{N/2}))/(\log N - \log N/2)$. This avoids the logarithmic correction in Eq. (F2).

[31] A. A. Nersesyan, A. M. Tsvelik, and F. Wenger, Disorder effects in two-dimensional d-wave superconductors, Physical Review Letters **72**, 2628 (1994).

[32] B. Sbierski, J. F. Karcher, and M. S. Foster, Spectrum-wide quantum criticality at the surface of class AIII topological phases: An "energy stack" of integer quantum Hall plateau transitions, Phys. Rev. X **10**, 021025 (2020).